Directed Self-Assembly of Poly(2-vinylpyridine)-*b*-polystyrene-*b*-poly(2-vinylpyridine) Triblock Copolymer with Sub-15 nm Spacing Line Patterns Using a Nanoimprinted Photoresist Template

Zhiwei Sun, Zhenbin Chen, Wenxu Zhang, Jaewon Choi, Caili Huang, Gajin Jeong, E. Bryan Coughlin, Yautzong Hsu, XiaoMin Yang, Kim Y. Lee, David S. Kuo, Shuaigang Xiao, and Thomas P. Russell**

There has been an increasing interest in preparing block copolymers (BCPs) thin films having lamellar microdomains oriented normal to the surface where the repeat period is small so as to achieve high areal densities.[1–5] Such materials would find broad application as templates for the fabrication of ultrahigh areal density nanowires,[6–9] bit-patterned media (BPM),[10,11] and graphene nanotransistors.[12,13] To obtain ultrasmall repeat periods, a large Flory–Huggins segmental interaction parameter (χ) is necessary to maintain a microphase separated morphology at low molecular weights. However, BCPs with large χ usually have marked differences in the surface energies between two blocks, making it difficult to orient the microdomains normal to the film surface. Usually, balanced interfacial interactions and surface energies are required to achieve this orientation, and different methods have been reported to balance the surface energies mismatch in high χ BCPs. Russell et al. reported the use of a surface-anchored random copolymer to balance the interfacial interactions of the blocks with the substrates.[14,15] Willson et al. reported the concept of the removable top coating polymer layer, which is neutral to BCP segment blocks, to balance the domain surface energies to obtain sub-20 nm spacing line patterns.[1,16] However, the design and removal of topcoat layer is delicate and complicated. Alternatively, solvent vapor annealing (SVA) can be used where surface energies and interfacial energies are mediated by the presence of the solvent. Morris and co-workers reported the use of a mixed solvent vapor annealing of PS-*b*-P4VP at elevated temperatures to orient lamellar microdomains normal to the surface and to achieve sub-15 nm domain spacing line patterns.[17] However, the high-temperature and long annealing times are undesirable. More facile and reliable routes to prepare ultrahigh density lamellar BCP perpendicular to substrate are needed.

Small domain spacing thin films could be obtained by reducing the degree of polymerization of the BCP, since the domain spacing varies as $D \approx \chi^{1/6} N^{2/3}$, where N is the total number of segments in the BCP.[18] However, as the molecular weight decreases, the BCPs will go to disordered state ($\chi N < 10.5$). Different methods have been reported to drive the disordered BCP into ordered state, while maintaining a small domain spacing, e.g., to increase χ_{eff} using hydrogen-bonded nanoparticles or small molecules, or chemical complexation of one block with a metal acid or salt.[19–24] Among these methods salt complexation is the simplest way to increase χ and induce ordering. As reported previously for metal ion complexed low molecular weight PS-*b*-PEO diblock copolymer, ordered BCP thin films with 7 nm pitch and 3 nm diameter cylindrical microdomains, corresponding to a 10 Terabit in.$^{-2}$ areal density.[25] It should also be noted that enhanced long-range lateral ordering and domain reorientation was achieved with salt complexation.[26]

Here, we prepared poly(2-vinylpyridine)-*b*-polystyrene-*b*-poly(2-vinylpyridine) (P2VP-*b*-PS-*b*-P2VP) triblock copolymer thin films with lamellae oriented normal to substrate using SVA. P2VP-*b*-PS-*b*-P2VP has good surface wetting characteristics and a large χ (0.18 at room temperature),[27] making it a promising candidate to generate high-density line patterns. Moreover, chelated with copper ions, P2VP blocks show an increased unfavorable interaction (χ_{eff}) with PS block, and drive the low molecular weight P2VP-*b*-PS-*b*-P2VP into ordered state, generating lamellar line patterns with sub-15 nm domain spacing. In addition, the directed self-assembly (DSA) of copper chloride doped P2VP-*b*-PS-*b*-P2VP triblock copolymer was carried out using nanoimprinted photoresist templates. As opposed to the time-consuming and costly electron beam lithography route,[28–35] NIL offers a simple, scalable route to replicate the topology from a master template. Moreover, the geometry parameters, e.g., line width and thickness, of the

Z. Sun, W. Zhang, J. Choi, C. Huang, G. Jeong, Prof. E. B. Coughlin, Prof. T. P. Russell
Department of Polymer Science and Engineering
University of Massachusetts Amherst
120 Governors Drive, Amherst, MA 01003, USA
E-mail: russell@mail.pse.umass.edu
Prof. Z. Chen
College of Materials Science and Engineering
Lanzhou University of Technology
Lanzhou 730050, Gansu, China
Dr. Y. Hsu, Dr. X. M. Yang, Dr. K. Y. Lee, Dr. D. S. Kuo, Dr. S. Xiao
Seagate Technology
LLD, 47010 Kato Road, Fremont, CA 94538, USA
E-mail: shuaigang.xiao@seagate.com

DOI: 10.1002/adma.201501585

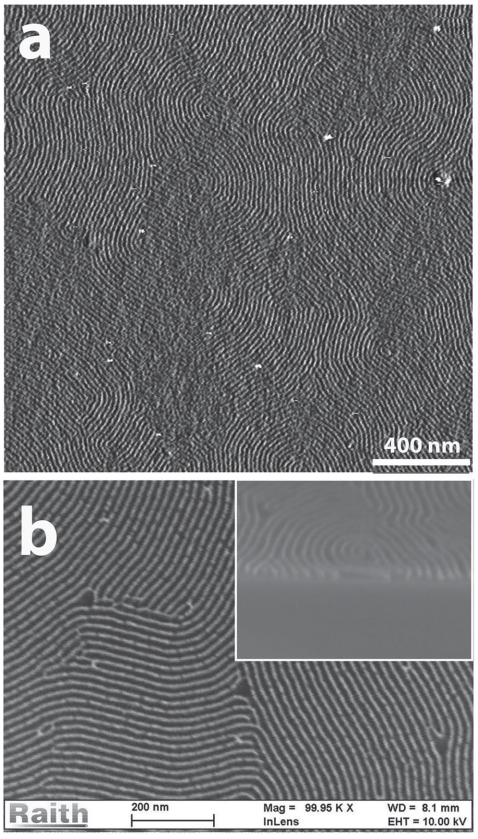

Figure 1. Line patterns obtained from perpendicularly oriented P2VP-*b*-PS-*b*-P2VP (47k) with 21.4 nm domain spacing. a) AFM phase image obtained after SVA in acetone vapor at room temperature; b) SEM image obtained after platinum salt infiltration and oxygen plasma exposure, inset is the corresponding cross-section image.

photoresist template could be fine tuned by oxygen plasma etching after nanoimprinting, offering a facile way to prepare defect free block copolymer nanopatterns with DSA.

We first prepared the perpendicular aligned lamellar P2VP-*b*-PS-*b*-P2VP with large molecular weight on neutral substrates by SVA according to literature procedures. [2] P(S-*r*-2VP-*r*-HEMA) random copolymers with a 2VP:PS unit ratio of ≈1:1 were anchored to the surface of the substrate to balance the BCP/substrate interfacial interactions. A 28 nm thick film of P2VP-*b*-PS-*b*-P2VP, with molecular weight of each block as 12k-*b*-23k-*b*-12k, or denoted as P2VP-*b*-PS-*b*-P2VP (47k), was spin coated onto the modified silicon wafer and a 21.4 nm pitch fingerprint pattern was obtained after annealing in acetone vapor for 30 min (**Figure 1**a). The solubility parameters of PS, P2VP, and acetone are 18.6, 21.7, and 20.3, respectively, so acetone is neutral to both PS and P2VP blocks, and BCP lamellae were oriented normal to substrate after SVA.[36] In order to enhance image contrast for electron microscopy, platinum metal nanowires were prepared by platinum salt infiltration and oxygen plasma treatment, a similar method reported by Chai et al.[37–39] Metal line patterns with a 21.4 nm pitch, which replicated the morphology of the BCP, were obtained after selective infiltration of platinum salt into the P2VP microdomains and removal of polystyrene using an oxygen plasma etching (Figure 1b). The cross-section of platinum nanowires, as shown in the inset of Figure 1b, indicated that BCP lamellae were oriented normal to the substrate through out the entire film (Figure S1, Supporting Information). Grazing incidence small-angle X-ray scattering (GISAXS) showed that domain spacing did not change after platinum salt infiltration (Figure S2, Supporting Information).

With the decreasing of molecular weight, P2VP-*b*-PS-*b*-P2VP (26k) with molecular weight of 6.7k-*b*-13k-*b*-6.7k was disordered when annealed in acetone (**Figure 2**a,c). While by introducing 10% copper chloride salt into the P2VP-*b*-PS-*b*-P2VP (26k) thin film, ordered line patterns with 16.4 nm spacing were obtained after SVA in acetone atmosphere (Figure 2b,d). Copper ions could be chelated with P2VP blocks, and increase the χ_{eff} between PS block and P2VP block, driving the otherwise phase mixed BCP into ordered state. Platinum line patterns were prepared after platinum salt infiltration and oxygen plasma etching (inset of Figure 2b).

The effect of salt concentration on BCP morphology was studied at low copper chloride concentrations (<20%). SEM images showed that ordered line patterns were obtained only when the copper ratio exceeded 10% with respect to P2VP repeat unit (Figure S3, Supporting Information). When the copper doping ratio was 10%, a sharp primary reflection at $q^* \approx 0.396$ nm^{-1} and a weak second-order reflection were observed at $2q^* \approx 0.79$ nm^{-1}, indicating ordered line patterns with domain spacing ≈15.9 nm ($2\pi/q^*$), in good agreement with the SEM and AFM data (Figure 2b). Lamellar line patterns still exist with copper-doping ratio as high as 14%. GISAXS showed that the q values of the primary scattering reflections decreased with increasing concentrations of copper chloride, corresponding to an increase in the domain spacing (Figure 2e). According to the literature, the immiscibility between two blocks increases linearly with salt concentration, that is:

$$\chi_{\text{eff}} = \chi_0 + mr \tag{1}$$

where χ_0 is Flory–Huggins segmental interaction parameter for the neat PS-*b*-P2VP-*b*-PS, r is the salt doping ratio, and m is a constant that depends on the BCP/salt pair.[24] Since the BCP microdomain spacing in the ordered state scales as $D \approx \chi_{\text{eff}}^{1/6}$ in the strong segregation regime, a linear relationship between domain spacing and salt ratio is predicted, as shown in Equation (2) assuming $mr/\chi_0 \ll 1$:

$$D = D'\left(\frac{\chi_{\text{eff}}}{\chi_0}\right)^{\frac{1}{6}} = D'\left(1+\frac{m}{\chi_0}r\right)^{\frac{1}{6}} \approx D'\left(1+\frac{m}{6\chi_0}r\right) \tag{2}$$

where D' is the virtual spacing of P2VP-*b*-PS-*b*-P2VP (26k) extrapolated to $r = 0$. The relationship between D and r using the GISAXS data (Figure 2f) in the strong segregation region ($r > 7\%$) fits well with Equation (2).

The behavior of the FWHM is rather interesting (Figure 2f). When the BCP is disordered, the FWHM decreases with increasing salt concentration, which is consistent with the BCP being disordered but approaching an ordering transition. At a 10%–11% copper salt doping ratio, the FWHM decreases dramatically, coupled with the appearance of very sharp reflections, indicating that the BCP has undergone an ordering

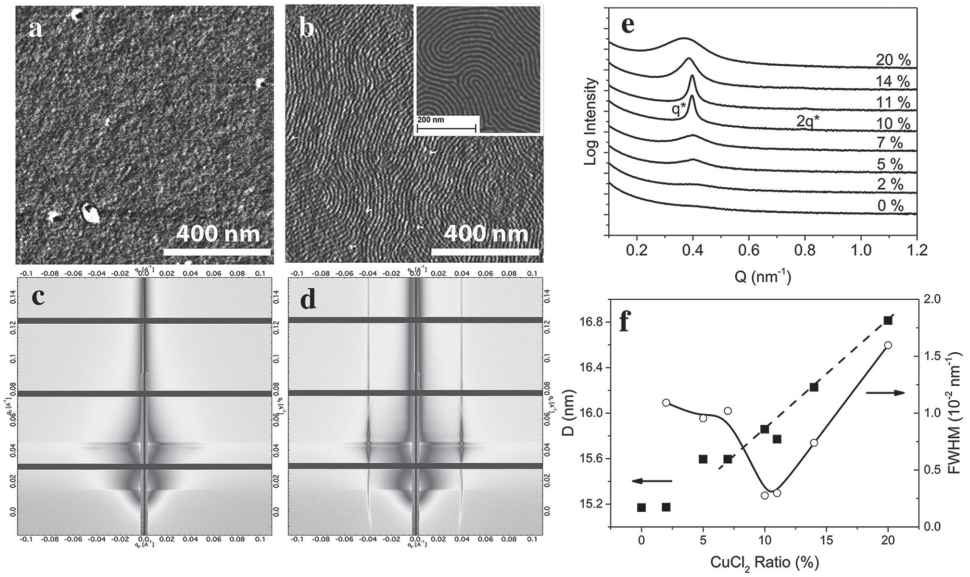

Figure 2. Effect of copper chloride doping on the morphology of P2VP-*b*-PS-*b*-P2VP (26k). a,c) AFM and GISAXS pattern of pure P2VP-*b*-PS-*b*-P2VP (26k) thin film after annealing; b,d) AFM and GISAXS pattern of P2VP-*b*-PS-*b*-P2VP (26k) with 10% copper chloride doping, inset in (b) is SEM image after "postannealing" platinum salt infiltration and removal of PS domain; e) intensity profile cut from GISAXS pattern of P2VP-*b*-PS-*b*-P2VP (26k) with different copper chloride doping ratios; f) the effect of copper chloride doping ratio on domain spacing (solid squares) and FWHM (open circles) of P2VP-*b*-PS-*b*-P2VP (26k) thin film.

transition and that a significant lateral ordering of the domains occurs. If more copper chloride is added, we would expect that the FWHM would continue to decrease but the reverse was seen. With increasing copper chloride concentration, the primary reflection broadens significantly, while the peak position continues to shift to smaller scattering vectors, i.e., the spacing continued to increase. This latter observation indicates that the stretching of the chains at the interface between the microdomains continues to increase with increasing copper chloride concentration, i.e., the segregation gets stronger or χ_{eff} increase. However, the increasing FWHM indicates that the grain size decreases and, when the copper ratio was 20%, no line patterns were observed. Rather, isolated dot structures without any ordering were found after acetone vapor annealing (Figure S3h, Supporting Information). These results suggest that for a copper doping ratio greater than 11%, χ_{eff} is so large that the reorganization of the microdomains is retarded or even prohibited. Consequently, a copper doping ratio of 10% was used for the remainder of the studies.

To obtain ultrasmall pitch lamellar line patterns, P2VP-*b*-PS-*b*-P2VP with much lower molecular weights were synthesized by RAFT polymerization using a dual functional initiator (Supporting Information). Fingerprint like line patterns with 14.1–16.6 nm domain spacing were obtained after copper chloride salt doping and acetone vapor annealing of P2VP-*b*-PS-*b*-P2VP films with molecular weight ranging from 20.8k to 25.2k (**Figure 3**a and Figure S4, Supporting Information). The

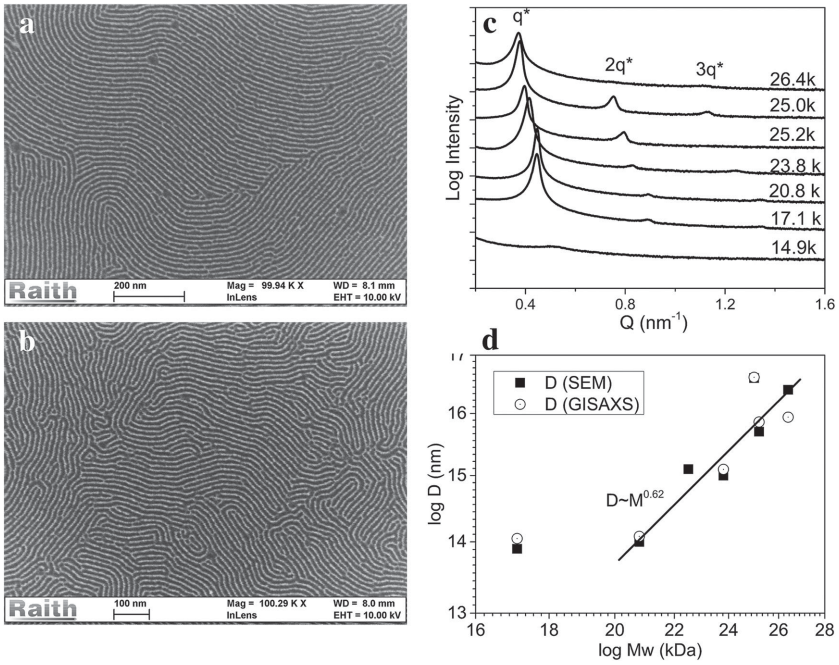

Figure 3. Effect of molecular weight on P2VP-*b*-PS-*b*-P2VP thin film domain spacing with 10% copper chloride doping. a) 14.1 nm platinum nanowires from P2VP-*b*-PS-*b*-P2VP(21k); b) 13.9 nm platinum nanowires from P2VP-*b*-PS-*b*-P2VP(17k); c) intensity profile cut from GISAXS pattern from of P2VP-*b*-PS-*b*-P2VP thin film with different molecular weights; d) the relationship between domain spacing and molecular weight of P2VP-*b*-PS-*b*-P2VP, solid squares are data from SEM images and open circles are data from GISAXS.

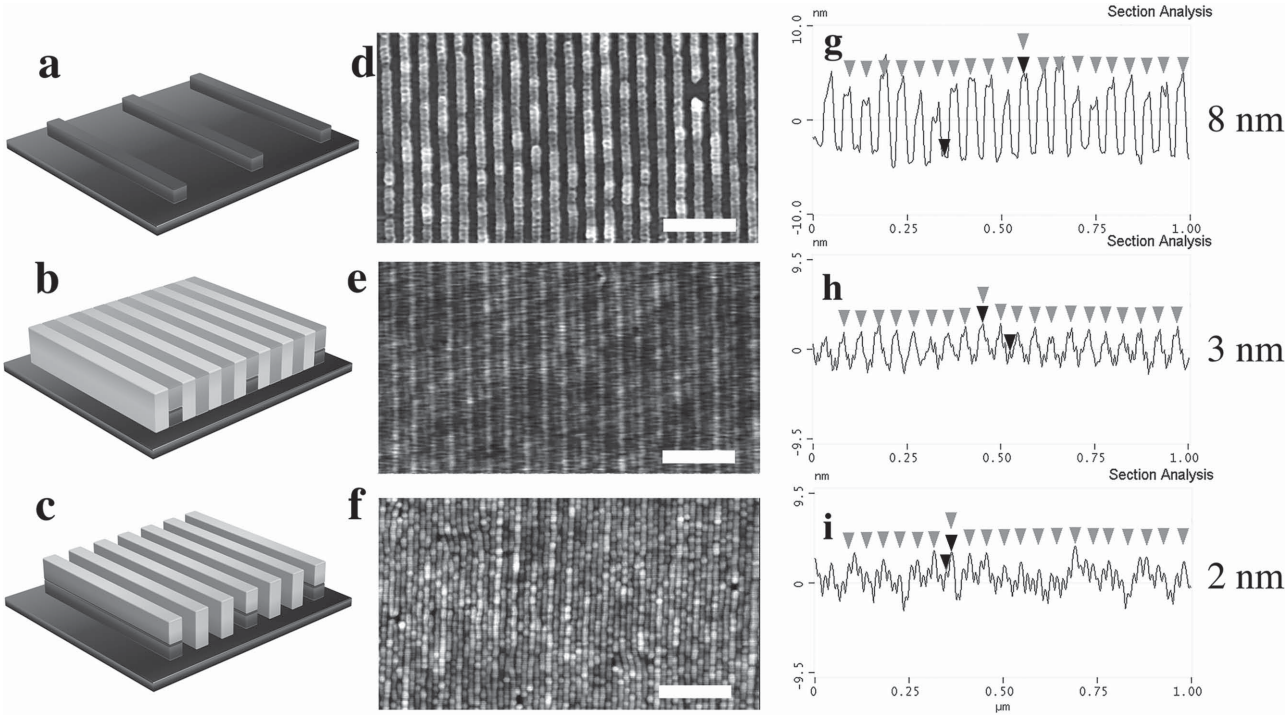

Figure 4. Schematics of directed self-assembly process of copper chloride doped P2VP-*b*-PS-*b*-P2VP (26k) on 50 nm pitch photoresist template. a) Nanoimprinted photoresist template after pretrimming; b) P2VP-*b*-PS-*b*-P2VP self-assembled on top of photoresist templates; c) platinum nanowires arrays prepared from P2VP-*b*-PS-*b*-P2VP thin film with ''postannealing" platinum salt infiltration and oxygen plasma exposure; d–f) AFM images of template in (a), block copolymer in (b), and metal line in (c), respectively; g–i) AFM height profiles of (d), (e), and (f), respectively; the gray triangle is where the photoresist stripes should be. The scale bars in AFM images are 200 nm.

primary peak of GISAXS profile shifted to larger q^* value with decreasing molecular weight, indicating that domain spacing decreased with decreasing molecular weight (Figure 3c). A plot of log (D) as a function of log (M_w) is shown in Figure 3d where an exponent of 0.62 is found albeit over a very limited range of molecular weight (from 20.8 to 26.4k). This exponent is consistent with the BCP being in the strong segregation regime ($D \approx M_w^{2/3}$).[18,41] Decreasing the molecular weight to 17.1k should have produced lamellae with a pitch of 12.5 nm theoretically, but the period was found to be 13.9 nm, much larger than expected (Figure 3b). We do not know the origin of this discrepancy and are currently investigating this. When the molecular weight of P2VP-*b*-PS-*b*-P2VP was decreased further, e.g., to 14.9k, the triblock copolymer remained disordered, regardless of the amount of copper chloride added (Figure 3c).

Various salts can be complexed with the P2VP and the choice of doping salt is important for obtaining high-quality ordered BCP films. P2VP-*b*-PS-*b*-P2VP agglomerates in solution, if doped with a strong interactive salt, e.g., multivalent zirconium (IV) chloride and tin (IV) chloride, preventing the preparation of uniform thin films. On the other hand, mono-valent salts, like lithium chloride, which have weak interactions with P2VP, are not strong enough to induce ordering in acetone SVA of P2VP-*b*-PS-*b*-P2VP thin films, even with up to a 20% doping ratio. However, Ryu and co-workers showed a clear disorder-to-order transition for PS-*b*-P2VP diblock copolymer with thermal annealing using lithium salt doping (LiCl and $LiClO_4$).[42] This discrepancy comes from the fact that χ_{eff} is weakly temperature dependent, while it is very sensitive to solvent uptake. The χ_{eff} of BCP with solvent swelling can be expressed in Equation (3), where ϕ_s is the volume ratio of solvent in BCP thin film and $\beta = 1.3–1.6$.[40,43]

$$\chi_{eff} = \chi_0(1-\phi_s)^{\beta} \quad (3)$$

According to Equation (3), the χ_{eff} decreases rapidly with increasing ϕ_s. So a relatively strong complexation salt is needed to maintain an ordered state during SVA. Copper (II) chloride has a mild interaction with P2VP, so homogeneous BCP/$CuCl_2$ premixed solution can be prepared, while its interaction is strong enough to induce ordering in the BCP thin film after SVA. The linear relationship between domain spacing and copper chloride doping ratio indicates a significant increase in χ_{eff}, counter-balancing the decrease of segmental interaction due to solvent swelling during SVA. Decreasing the domain spacing beyond 14 nm, however, requires a combination of salt doping and new BCPs with even a larger intrinsic χ parameter.

The DSA of lamellae-forming P2VP-*b*-PS-*b*-P2VP with copper chloride doping was studied using templates prepared by nanoimprint lithography (NIL), and long-range laterally ordered lamellar line patterns with ultrahigh areal density were prepared on sparsely patterned photoresist templates. Studies were first performed using P2VP-*b*-PS-*b*-P2VP (26k), which was microphase separated into 16.4 nm lamellar line patterns with 10% copper chloride doping. The photoresist template prepared with NIL was trimmed using oxygen plasma etching for 30 s prior to BCP thin film was coated and SVA was applied. **Figure 4** shows a 3× density multiplication of the line pattern using DSA on a

50 nm pitch photoresist template with 8 nm thickness (Figure 4d). The evolution of the surface topology was measured using AFM before and after DSA (Figure 4d–f). After SVA with acetone, the BCP was self-assembled along the direction of photoresist strips (Figure 4b,e,h). A peak-valley height difference of about 3 nm with a pitch of 50 nm was originated from the modulation from the template (Figure 4e,h), as observed after SVA. It is difficult to distinguish individual PS or P2VP domains between photoresist stripes in Figure 4e, due to the fact that the topology contrast between different domains was really small. While long-range ordered platinum nanowires with 16.7 nm pitch, which is three times the line density of the photoresist template, were observed after platinum salt/acid infiltration and oxygen plasmas exposure (Figure 4f). The background modulation originated from the template topology was still preserved in the metal lines arrays (Figure 4c,f,i), where every two metal lines were interspaced by one with higher topology (gray triangles in Figure 4i). This difference may arise from the fact that one metal line was located on top of the photoresist stripes defining the trench, while the other two lower lines were located within the trench (Figure 4c). Based on this observation, we predicted a mechanism of DSA using the photoresist template. The photoresist strips after oxygen plasma etching might be preferentially wetted by P2VP domains due to its high polarity after oxidation, and there were another two P2VP domains and three alternating PS domains located in between of the adjacent photoresist stripes (Figure 4b). Line density was multiplied by three times after DSA compared with its original photoresist template.

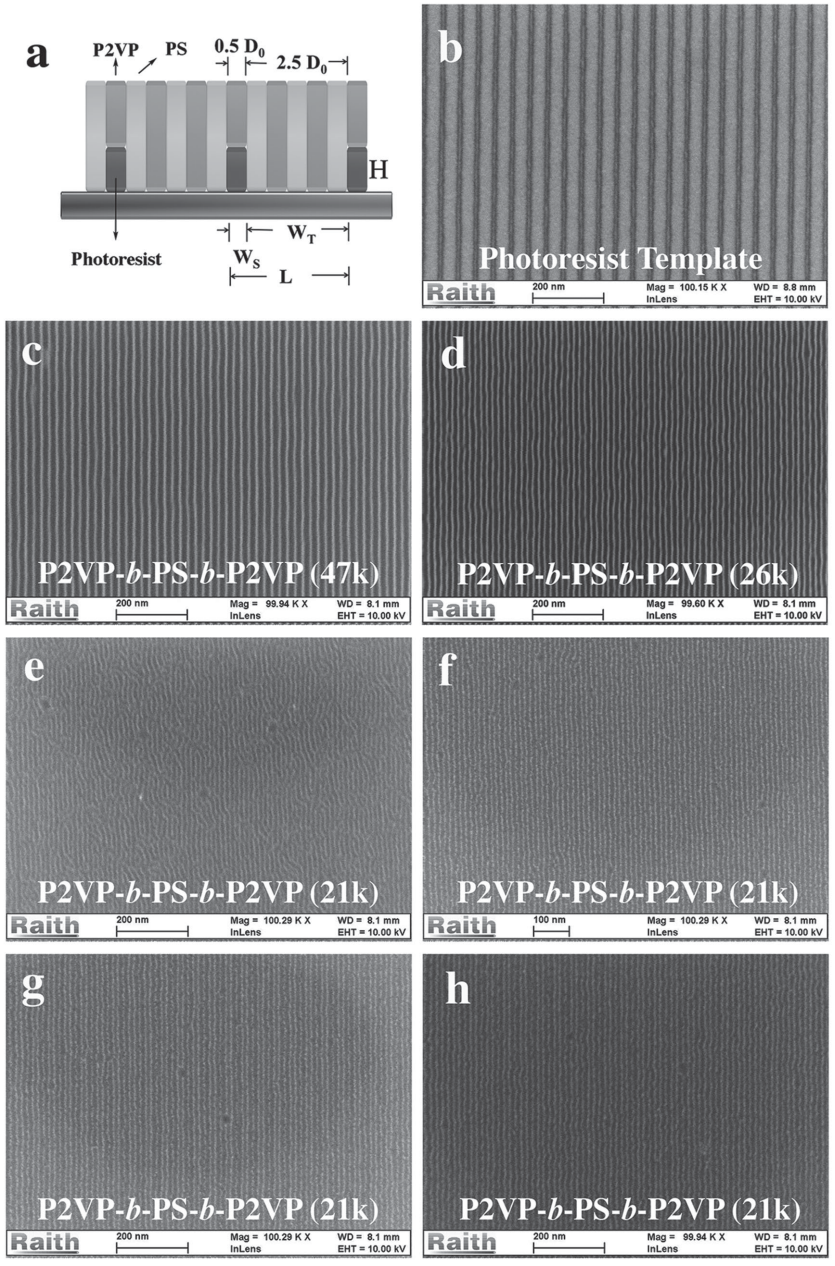

Figure 5. Platinum nanowires arrays prepared from long-range ordered P2VP-*b*-PS-*b*-P2VP on photoresist templates with different pitches. a) Ideal geometric commensurate model for three-time density amplification DSA, where blue is photoresist stripes, pink and green are P2VP domain and PS domain, respectively; b) photoresist template, with L = 50 nm, H = 8 nm, W_S = 11 nm, and W_T = 39 nm; c) 21.5 nm domain P2VP-*b*-PS-*b*-P2VP (47k) self-assembled on 43 nm pitch template; d) copper chloride doped P2VP-*b*-PS-*b*-P2VP (26k) with 16.7 nm spacing self-assembled on 50 nm pitch template as shown in (b); e–h) copper chloride doped P2VP-*b*-PS-*b*-P2VP (21k) self-assembled on 42, 44, 46, and 48 nm pitch templates, respectively, with $D = 1/3L$.

The geometry of the template is critical for high-quality DSA of BCPs. There are four important geometric parameters for nanoimprinted photoresist templates; the pitch, photoresist thickness (H), the width of photoresist stripes (W_S), and the width of the trench between two stripes (W_T), where $L = W_S + W_T$ (**Figure 5**a). We first studied the effect of photoresist thickness (H) on the quality of DSA with P2VP-*b*-PS-*b*-P2VP (26k) on nanoimprinted photoresist templates with L = 50 nm. The initial template thickness after NIL was ≈35 nm (H_0) (Figure S5 and S6, Supporting Information). Prior to coating with the BCP, oxygen plasma was used to pretrim the photoresist template. The photoresist thickness H decreased almost linearly with increasing etching time (Figure S7, Supporting Information). High-quality DSA patterns were obtained on photoresist templates with H = 8–10 nm (Figure 5d). Neither thicker nor thinner templates improved the DSA pattern, e.g., the template with 3 or 26 nm photoresist thickness did not guide P2VP-*b*-PS-*b*-P2VP microdomains as well as the templates with 8 nm thickness (Figure S7, Supporting Information).

Defect-free DSA usually requires commensurability between the template pitch (L) and BCP period (D_0) where L/D_0 is

an integral; e.g., high-quality line patterns were obtained by directing the assembly of P2VP-*b*-PS-*b*-P2VP (47k, $D_0 = 21.5$ nm) on 43 nm pitch photoresist template (Figure 5c), or by directing salt-doped P2VP-*b*-PS-*b*-P2VP (26k, $D_0 = 16.4$ nm) with 50 nm pitch photoresist template (Figure 5d). However, P2VP-*b*-PS-*b*-P2VP (21k, $D_0 = 14.1$ nm), blended with 10% copper chloride, showed numerous dislocations on pitch commensurate templates ($L = 42$ nm, Figure 5e). The origin of this can be that the photoresist stripe width (W_S) and trench width (W_T) in the 42 nm pitch photoresist template were incommensurate with D_0. As discussed previously, one P2VP domain stood on top of the photoresist stripes and the remaining two and a half-domain spacing were constrained in the trench between two photoresist stripes. Consequently, the ideal geometry for a 3× density amplification would be $W_S = 0.5 \times D_0$, $W_T = 2.5 \times D_0$, and $L = 3 \times D_0$. The photoresist stripe widths of all templates used in this study were controlled to be the same, namely at $W_S = 11$ nm (Figure 5b), which means $W_T = L - W_S = 31$ nm for 42 nm pitch photoresist template. The trench width W_T is 4 nm smaller than the required 35 nm ($2.5 \times D_0 = 35$ nm) for the P2VP-*b*-PS-*b*-P2VP (21k, $D_0 = 14.1$ nm) to fit precisely and numerous defects were introduced due to confinement effects. If the template pitch is larger than 44 nm, there will be trenches with width more than 33 nm, which is close to 2.5 periods of the BCP, so constraints are relaxed and defect density decreases significantly (Figure 5f–h). Moreover, the spacing of the BCP on the incommensurate template was stretched to accommodate the incommensurability, namely 1/3 of the template pitch, i.e., P2VP-*b*-PS-*b*-P2VP (21k) was stretched from 14.1 to 14.5 nm, 15.2 and 16.0 nm on 44, 46, and 48 nm pitch template, respectively (Figure 5f–h). When the template pitch was increased to 50 nm, the BCP spacing was ≈16.2 nm as measured by SEM, slightly smaller than 1/3 of the template pitch (16.7 nm), which suggests a maximum stretching of the P2VP-*b*-PS-*b*-P2VP (21k) chains of nearly 15% (Figure S8, Supporting Information). An explanation for domain spacing expansion is that PS middle blocks in the triblock copolymer bridge between two adjacent P2VP lamellar domains, enabling significant stretching.[41,44] It should be noted that similar types of BCP domain stretching were observed by Russell,[45] Ross,[46] and recently by Nealey[47] and their co-workers on incommensurate templates.

In summary, we report a simple way to prepare sub-15 nm domain spacing line patterns from low molecular weight lamellae-forming P2VP-*b*-PS-*b*-P2VP with copper chloride doping. Copper ions were selectively complexed with the P2VP block, and drove the block copolymer into the ordered state. High areal density BCP thin films with enhanced lateral ordering were obtained by complexation with 10% copper chloride. P2VP-*b*-PS-*b*-P2VP thin films prepared with salt doping and SVA were compatible with DSA using photoresist templates prepared by NIL. Long-range ordered thin films with 14 nm domain spacing line patterns were prepared over large area on photoresist templates, which could be a potential etching mask for pattern transfer onto hard substrates.

Experimental Section

Materials: Lamellae-forming P2VP-*b*-PS-*b*-P2VP with different molecular weights were either obtained from Polymer Source, Inc, or synthesized by RAFT polymerization with a dual functional chain transfer agent (Figure S9–S11, Supporting Information), with PDI < 1.3, and styrene/vinyl pyridine mole ratio close to 1:1. The poly(styrene-*ran*-2-vinylpyridine-*ran*-hydroxylethyl methacrylate) random copolymer (P(S-*r*-2VP-*r*-HEMA)) was synthesized according to the literature.[4] The molecular weight, PDI, and chemical compositions of all polymers used here are listed in Table S1 in the Supporting Information. Copper (II) chloride anhydrous from Acros Organics and sodium tetrachloroplatinate (II) hydrate from Sigma-Aldrich were used as received.

Block Copolymer Thin Film Preparation: $CuCl_2$ was premixed with BCP in solutions by blending P2VP-*b*-PS-*b*-P2VP/toluene solution and $CuCl_2$/THF solution and stayed overnight to equilibrium before use. Block copolymer thin films were coated onto P(S-*r*-2VP-*r*-HEMA) grafted silicon substrates, and then were annealed in acetone vapor environment for 30 min in a chamber with nitrogen inlet and outlet which were reported in our previous work.[48] The film thicknesses of BCP in swollen state were controlled to be 150% by fine-tuning the nitrogen flow rate.

Preparation of Photoresist Template for DSA: 6 in. quartz NIL master molds with 40–50 nm pitches in 1 nm increment were prepared using rotary electron beam lithography system (Elionix). UV crosslinking Photoresist FT247 from Molecular Imprints was drop-dispensed on 6 in. silicon wafer and the quartz NIL master mold was applied on the top of resist. Photoresist was exposed to UV light during the printing, creating line prepatterns in a 35 nm thick photoresist film after crosslinking. The photoresist prepatterns replicated the geometry of the quartz NIL master mold prepared with electron beam lithography, with an initial 16 nm line width and 35 nm line thickness (Figure S5a and S6a, Supporting Information). Then, photoresist template was trimmed using oxygen plasma before coating of BCP, using an Oxford PlasmaLab 100 reactive ion etching system. The etching parameters were 2 mTorr pressure, 30 W forward power, and 30 sccm oxygen plasma flow rate. Both the width and thickness of photoresist lines were decreased during oxygen plasma trimming (Figure S5–S7, Supporting Information). The template geometry was optimized for DSA by 30 s oxygen plasma trimming (Figure S5b, S6b, and S7b, Supporting Information). BCP thin films were then coated on photoresist templates and were annealed in acetone vapor for 30 min to get ordered. Long-range ordered platinum lines were prepared after Na_2PtCl_4 salt infiltration and oxygen plasmas etching.

Preparation of Platinum Nanowires: Platinum nanowires were prepared according to the literature.[37,38] Ordered P2VP-*b*-PS-*b*-P2VP thin films after SVA were immersed in 20 mg mL^{-1} Na_2PtCl_4 aqueous solution with 0.9 wt% HCl. Platinum salt/acid will selectively infuse into the P2VP microdomains. Then, oxygen plasma was used to remove the BCP and the platinum salt was reduced to metallic platinum nanowires during plasma etching.

Grazing Incidence Small Angle X-Ray Scattering: GISAXS were measured in Advanced Light Source (ALS) Beamline 7.3.3 in Lawrence Berkeley National Laboratory. The beam energy was 10 keV with wavelength of 0.124 nm. The incident angle was 0.16°.

Supporting Information

Supporting Information is available from the Wiley Online Library or from the author.

Acknowledgements

Z.S. and Z.C. contributed equally to this work. This work was supported by Seagate Technologies and the NSF-Supported Center for Hierarchical Manufacturing (CMMI-1025020) at the University of Massachusetts. The authors acknowledge the use of Beamline 7.3.3 at Advanced Light Source, Berkeley National Laboratory, which is supported by the Office of Science, Office of Basic Energy Sciences, of the US Department of Energy. E.B.C. and W.Z. were supported by the US Army MURI

on Ion Transport in Complex Heterogeneous Organic Materials (W911NF-10-1-0520).

Received: April 2, 2015
Revised: April 24, 2015
Published online: June 18, 2015

[1] C. M. Bates, T. Seshimo, M. J. Maher, W. J. Durand, J. D. Cushen, L. M. Dean, G. Blachut, C. J. Ellison, C. G. Willson, *Science* **2012**, *338*, 775.
[2] G. S. Khaira, J. Qin, G. P. Garner, S. Xiong, L. Wan, R. Ruiz, H. M. Jaeger, P. F. Nealey, J. J. de Pablo, *ACS Macro Lett.* **2014**, *3*, 747.
[3] H. Yoshida, H. S. Suh, A. Ramirez-Herunandez, J. I. Lee, K. Aida, L. Wan, Y. Ishida, Y. Tada, R. Ruiz, J. de Pablo, P. F. Nealey, *J. Photopolym. Sci. Technol.* **2013**, *26*, 55.
[4] S. Ji, C.-C. Liu, J. G. Son, K. Gotrik, G. S. W. Craig, P. Gopalan, F. J. Himpsel, K. Char, P. F. Nealey, *Macromolecules* **2008**, *41*, 9098.
[5] J. G. Kennemur, L. Yao, F. S. Bates, M. A. Hillmyer, *Macromolecules* **2014**, *47*, 1411.
[6] T. Thurn-Albrecht, J. Schotter, G. A. Kästle, N. Emley, T. Shibauchi, L. Krusin-Elbaum, K. Guarini, C. T. Black, M. T. Tuominen, T. P. Russell, *Science* **2000**, *290*, 2126.
[7] R. A. Farrell, N. T. Kinahan, S. Hansel, K. O. Stuen, N. Petkov, M. T. Shaw, L. E. West, V. Djara, R. J. Dunne, O. G. Varona, P. G. Gleeson, S.-J. Jung, H.-Y. Kim, M. M. Kolesnik, T. Lutz, C. P. Murray, J. D. Holmes, P. F. Nealey, G. S. Duesberg, V. Krstic, M. A. Morris, *Nanoscale* **2012**, *4*, 3228.
[8] B. H. Kim, D. H. Lee, J. Y. Kim, D. O. Shin, H. Y. Jeong, S. Hong, J. M. Yun, C. M. Koo, H. Lee, S. O. Kim, *Adv. Mater.* **2011**, *23*, 5618.
[9] S.-J. Jeong, H.-S. Moon, J. Shin, B. H. Kim, D. O. Shin, J. Y. Kim, Y.-H. Lee, J. U. Kim, S. O. Kim, *Nano Lett.* **2010**, *10*, 3500.
[10] S. Xiao, X. Yang, P. Steiner, Y. Hsu, K. Lee, K. Wago, D. Kuo, *ACS Nano* **2014**, *8*, 11854.
[11] R. Ruiz, H. Kang, F. A. Detcheverry, E. Dobisz, D. S. Kercher, T. R. Albrecht, J. J. de Pablo, P. F. Nealey, *Science* **2008**, *321*, 936.
[12] G. Liu, Y. Wu, Y.-M. Lin, D. B. Farmer, J. A. Ott, J. Bruley, A. Grill, P. Avouris, D. Pfeiffer, A. A. Balandin, C. Dimitrakopoulos, *ACS Nano* **2012**, *6*, 6786.
[13] B. H. Kim, J. Y. Kim, S.-J. Jeong, J. O. Hwang, D. H. Lee, D. O. Shin, S.-Y. Choi, S. O. Kim, *ACS Nano* **2010**, *4*, 5464.
[14] E. Huang, T. P. Russell, C. Harrison, P. M. Chaikin, R. A. Register, C. J. Hawker, J. Mays, *Macromolecules* **1998**, *31*, 7641.
[15] G. J. Kellogg, D. G. Walton, A. M. Mayes, P. Lambooy, T. P. Russell, P. D. Gallagher, S. K. Satija, *Phys. Rev. Lett.* **1996**, *76*, 2503.
[16] E. Kim, W. Kim, K. H. Lee, C. A. Ross, J. G. Son, *Adv. Funct. Mater.* **2014**, *24*, 6981.
[17] A. Chaudhari, T. Ghoshal, M. T. Shaw, C. Cummins, D. Borah, J. D. Holmes, M. A. Morris, *Proc. SPIE* **2014**, *9051*, 905110.
[18] Y. Matsushita, K. Mori, R. Saguchi, Y. Nakao, I. Noda, M. Nagasawa, *Macromolecules* **1990**, *23*, 4313.
[19] J.-Y. Wang, W. Chen, C. Roy, J. D. Sievert, T. P. Russell, *Macromolecules* **2008**, *41*, 963.
[20] J.-Y. Wang, W. Chen, T. P. Russell, *Macromolecules* **2008**, *41*, 4904.
[21] S. H. Kim, M. J. Misner, L. Yang, O. Gang, B. M. Ocko, T. P. Russell, *Macromolecules* **2006**, *39*, 8473.
[22] S. Naidu, H. Ahn, J. Gong, B. Kim, D. Y. Ryu, *Macromolecules* **2011**, *44*, 6085.
[23] A. A. Teran, N. P. Balsara, *J. Phys. Chem. B* **2013**, *118*, 4.
[24] W.-S. Young, T. H. Epps, *Macromolecules* **2009**, *42*, 2672.
[25] S. Park, D. H. Lee, J. Xu, B. Kim, S. W. Hong, U. Jeong, T. Xu, T. P. Russell, *Science* **2009**, *323*, 1030.
[26] J. He, J. Y. Wang, J. Xu, R. Tangirala, D. Shin, T. P. Russell, X. Li, J. Wang, *Adv. Mater.* **2007**, *19*, 4370.
[27] K. H. Dai, E. J. Kramer, *Polymer* **1994**, *35*, 157.
[28] A. Tavakkoli, K. G, K. W. Gotrik, A. F. Hannon, A. Alexander-Katz, C. A. Ross, K. K. Berggren, *Science* **2012**, *336*, 1294.
[29] J.-B. Chang, J. G. Son, A. F. Hannon, A. Alexander-Katz, C. A. Ross, K. K. Berggren, *ACS Nano* **2012**, *6*, 2071.
[30] J.-B. Chang, H. K. Choi, A. F. Hannon, A. Alexander-Katz, C. A. Ross, K. K. Berggren, *Nat. Commun.* **2014**, *5*, 3305.
[31] J. K. W. Yang, Y. S. Jung, J.-B. Chang, R. A. Mickiewicz, A. Alexander Katz, C. A. Ross, K. K. Berggren, *Nat. Nanotechnol.* **2010**, *5*, 256.
[32] C. A. Ross, K. K. Berggren, J. Y. Cheng, Y. S. Jung, J.-B. Chang, *Adv. Mater.* **2014**, *26*, 4386.
[33] J. G. Son, M. Son, K.-J. Moon, B. H. Lee, J.-M. Myoung, M. S. Strano, M.-H. Ham, C. A. Ross, *Adv. Mater.* **2013**, *25*, 4723.
[34] X. Liang, S. Wi, *ACS Nano* **2012**, *6*, 9700.
[35] S.-M. Park, X. Liang, B. D. Harteneck, T. E. Pick, N. Hiroshiba, Y. Wu, B. A. Helms, D. L. Olynick, *ACS Nano* **2011**, *5*, 8523.
[36] J. Brandrup, *Polymer Handbook*, 4th ed., Wiley, New York 1999.
[37] J. Chai, D. Wang, X. Fan, J. M. Buriak, *Nat. Nanotechnol.* **2007**, *2*, 500.
[38] J. Chai, J. M. Buriak, *ACS Nano* **2008**, *2*, 489.
[39] J. G. Lee, Y. S. Jung, S.-H. Han, K.-M. Kim, Y.-K. Han, *Adv. Mater.* **2014**, *26*, 2894.
[40] T. P. Lodge, C. Pan, X. Jin, Z. Liu, J. Zhao, W. W. Maurer, F. S. Bates, *J. Polym. Sci., Part B: Polym. Phys.* **1995**, *33*, 2289.
[41] M. W. Matsen, M. Schick, *Macromolecules* **1994**, *27*, 187.
[42] B. Kim, H. Ahn, J. H. Kim, D. Y. Ryu, J. Kim, *Polymer* **2009**, *50*, 3822.
[43] T. P. Lodge, K. J. Hanley, B. Pudil, V. Alahapperuma, *Macromolecules* **2003**, *36*, 816.
[44] M. W. Matsen, *J. Chem. Phys.* **1995**, *102*, 3884.
[45] P. Lambooy, T. P. Russell, G. J. Kellogg, A. M. Mayes, P. D. Gallagher, S. K. Satija, *Phys. Rev. Lett.* **1994**, *72*, 2899.
[46] J. Y. Cheng, C. A. Ross, E. L. Thomas, H. I. Smith, G. J. Vancso, *Adv. Mater.* **2003**, *15*, 1599.
[47] S. Ji, U. Nagpal, G. Liu, S. P. Delcambre, M. Müller, J. J. de Pablo, P. F. Nealey, *ACS Nano* **2012**, *6*, 5440.
[48] X. Gu, I. Gunkel, A. Hexemer, W. Gu, T. P. Russell, *Adv. Mater.* **2014**, *26*, 273.